UC Irvine
UC Irvine Previously Published Works

Title
A spectrally splitting photovoltaic-thermal hybrid receiver utilising direct absorption and wave interference light filtering

Permalink
https://escholarship.org/uc/item/4wq7d36p

Authors
Mojiri, Ahmad
Stanley, Cameron
Taylor, Robert A
et al.

Publication Date
2015-08-01

DOI
10.1016/j.solmat.2015.03.011

Copyright Information
This work is made available under the terms of a Creative Commons Attribution License, availalbe at https://creativecommons.org/licenses/by/4.0/

Peer reviewed

eScholarship.org Powered by the California Digital Library
University of California

Solar Energy Materials & Solar Cells 139 (2015) 71–80

Contents lists available at ScienceDirect

Solar Energy Materials & Solar Cells

journal homepage: www.elsevier.com/locate/solmat

A spectrally splitting photovoltaic-thermal hybrid receiver utilising direct absorption and wave interference light filtering

Ahmad Mojiri [a], Cameron Stanley [a], Robert A. Taylor [b], Kourosh Kalantar-zadeh [c], Gary Rosengarten [a,*]

[a] School of Aerospace, Mechanical, and Manufacturing Engineering, RMIT University, Melbourne, VIC 3001, Australia
[b] School of Mechanical and Manufacturing Engineering, School of Photovoltaics and Renewable Energy Engineering, University of New South Wales, Kensington, New South Wales 2052, Australia
[c] School of Electrical and Computer Engineering, RMIT University, Melbourne, Victoria 3053, Australia

ARTICLE INFO

Article history:
Received 1 September 2014
Received in revised form
13 January 2015
Accepted 11 March 2015
Available online 1 April 2015

Keywords:
Solar
Concentrating
Hybrid
Spectral splitting
Spectral modification

ABSTRACT

We have developed a novel spectrally splitting hybrid solar receiver by combining a simple dichroic filter and a liquid channel as a selective absorbing medium. The combination acts as a band pass filter for silicon solar cells. The geometry can be optimised for any linear concentrator; in this paper we have optimised it for a commercially available linear rooftop micro-concentrator. The optics of the concentrator at its focal region has been investigated using ray tracing. A simple 5-layer dichroic filter made of titanium dioxide and silicon dioxide has been designed, optimised, and fabricated with a focus placed on manufacturing simplicity. It has been shown that such a filter directs 54.5% of the concentrated light to the silicon photovoltaic cells; the Si cells considered in this paper can convert 26.1% of this energy into electricity which is significantly higher than their 20.6% efficiency under the full spectrum. This is due to the fact that 73.3% of the incident flux is within the cell's relatively high spectral response range, which can be efficiently converted into electricity. The rest of the spectrum can be collected as high temperature heat. This research shows the possibility of employing low-cost direct absorption-dichroic filtering hybrid receivers in liner concentrators.

© 2015 Elsevier B.V. All rights reserved.

1. Introduction

Increasing the efficiency of solar receivers represents a desirable pathway towards reducing the installed cost per Watt, and obtaining higher solar fractions in buildings with limited rooftop areas. Concentrating photovoltaic (CPV) systems and hybrid photovoltaic-thermal receivers can help us to achieve this. High heat loads in CPV systems are considered an opportunity to design a combined heat and power system to deliver electricity and heat concurrently.

Three main methods have been introduced to remove heat from CPV systems: (a) thermal removal, through passively or actively cooled cells [1], (b) device removal, through the use of high efficiency multi-junction cells [2], and (c) optical removal, through spectral modification of the incoming sunlight [3,4]. A combination of these methods can also be incorporated to achieve the best outcome [5]. In the third method, sunlight is separated into two or more spectral bands with each band directed towards an appropriate receiver. For example, the most suitable spectral band for silicon cells as the most common type of PV cells is roughly between 700 nm and 1100 nm [6]. Using spectral beam splitting in concentrating photovoltaic thermal receivers (CPVT) can not only improve the total efficiency [3] of the system but also thermally decouple the thermal receiver from the cell. The latter allows the temperature of the thermal output to increase beyond the maximum operational temperature of the PV cell and to deliver high grade high temperature thermal output in addition to electricity. This may improve the market penetration of solar energy in solar cooling and industrial applications.

Application of spectral beam splitting in solar energy has been extensively studied for CPV systems, e.g. Barnett and Wang [7] designed and optimised a spectral beam splitting PV system using dichroic filtering for GaInP/GaAs, Si, and GaInAsP/GaInAs cells achieving an efficiency of 39.1% at a concentration ratio (CR) of 30. Khvostikov et al. [8] proposed dichroic filtering in combination with AlGaAs, GaAs, GaSb reaching an efficiency of 39.6%. The outcome of the research in this field has been reviewed thoroughly in [3,4]. Applying spectral splitting in CPVT systems has been studied by Chendo et al. [9] and Hamdy and Osborn [10] in detail. They analysed the system performance over the year and

* Corresponding author. Tel.: +61 3 9925 8020.
E-mail address: gary.rosengarten@rmit.edu.au (G. Rosengarten).

http://dx.doi.org/10.1016/j.solmat.2015.03.011
0927-0248/© 2015 Elsevier B.V. All rights reserved.

showed that the reduced heat load on the PV cells improves the electric conversion efficiency of the system. Recently Jiang et al. [11] studied a CPVT parabolic trough system using dichroic filters with 240–400 °C thermal output. However the majority of research in this field is limited to theoretical analyses with a few practical realisation. These devices have been too expensive to be commercially viable for linear concentrators. Wave interference [12,13] and selective absorption [9] filters can be used for spectral separation in CPVT systems. Wave interference filters employ a number of high and low refractive index transparent materials (multilayer thin film filters) or a transparent layer with continuously varying refractive index (rugate filters) deposited on a substrate to generate the light filtering effect. Selective absorbers use pure liquids, solution mixtures [9,14], nano-fluids [15,16], or solid state optical filters to filter out the desired spectral band(s).

Wave interference filters provide more flexibility compared to selective absorbers [12]. Such filters can be broad band-pass which are made of one or two edge filters in combination. These two edge filters (a long and a short pass) can be deposited on either side of a substrate. A concern in such band pass filters is to combine them in such a way that one edge filter does not create transmission peaks in the rejection band of the other [17]. However, they normally consist of a large number of layers to produce an effective broadband filtering effect, but this results in higher cost.

In this work, we propose a hybrid photovoltaic-thermal (CPVT) receiver in a linear Fresnel concentrator incorporating a selective absorber together with a wave interference filter (a dichroic mirror), acting as a band pass filter. A simple filtering structure that is introduced is relatively facile and low cost to manufacture. The proposed configuration takes advantage of direct solar absorption that has been studied by Minradi [18] and Otanicar [19,20] to simplify the structure of the required dichroic coating. The details of the design are given in the next section where we present an optical analysis of the whole system and discuss the advantages of using the proposed configuration.

2. Design description

In this paper, the term hybrid collector refers to the combination of a rooftop linear micro-concentrator (LMC) and a CPVT receiver installed at its focal axis. In this section, we briefly introduce the proposed hybrid receiver design and then discuss its applicability in an LMC hybrid collector.

2.1. The hybrid receiver design

The proposed hybrid receiver consists of a high temperature (above 150 °C) liquid channel optically coupled to high efficiency back contact crystalline silicon (Si) cells that have been optimised for concentrating photovoltaic (CPV) applications [21]. The overall configuration of the receiver is shown in Fig. 1. Concentrated light propagates in the upward direction and enters the receiver through the front glass. It passes through this highly transparent glass and enters the semi-transparent liquid flowing inside the channel. The liquid serves as a heat transfer fluid as well as a spectral filter. Vivar and Everett [14] have provided a review on optical and heat transfer properties of a range of liquids for such an application. Candidate liquids considered in this paper are water, propylene glycol, and ethylene glycol. The optical properties of these liquids will be discussed in the following sections.

The liquid channel acts as a short pass filter with a cut-off wavelength at near infrared, e.g. 1200 nm. Shorter wavelengths first pass through both the liquid and the highly transparent rear glass with negligible attenuation, and then land on the dichroic coating at the top face of the rear glass. This coating acts as a long pass filter, reflecting all wavelengths shorter than 600 nm and transmitting the remainder of the spectrum. The reflected and transmitted rays are absorbed by the absorbing side walls and the PV cells, respectively. The silicone layer between the rear glass and PV cells is required to achieve a better refractive index match between the various layers to minimise the reflection losses. It also provides a high thermal resistance between the hot channel and the PV cells.

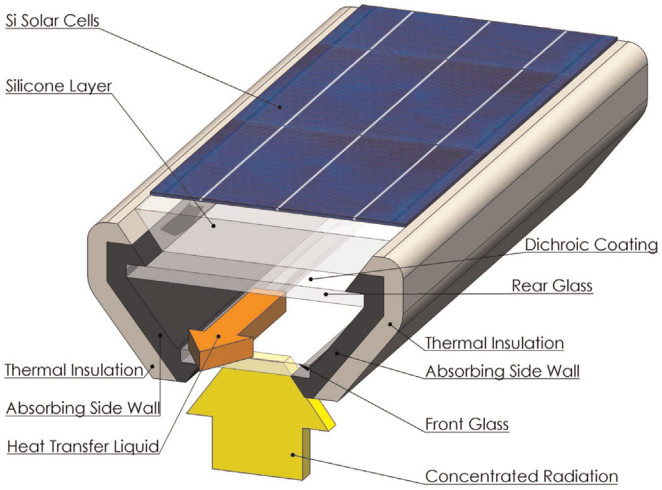

Fig. 1. Concentrated light enters the receiver through the front glass and is filtered by the dichroic coating at the top side of the rear glass. The filtered light is sent to the PV cells and the rest is absorbed by the side walls or directly in the fluid.

The absorbing side walls are made of metal for better heat transfer across the wall with a highly absorbing coating on their surface. It is important to note that this surface does not need to be a selective surface because it is in direct contact with the liquid layer that absorbs all infrared thermal emission from the hot surface. The outside of the absorbing side walls is thermally insulated.

3. Methods

3.1. The rooftop linear micro-concentrator (LMC)

The LMC is a one-axis solar tracking concentrator developed and commercialised by Chromasun Pty Ltd [22–24]. It comprises two sets of Fresnel reflectors, each set with 10 curved mirrors, encapsulated inside a glass canopy. The mirrors are controlled by a tracking system to focus the sunlight on a central axis 25 cm above the mirror plane. The whole collector is 3.3 m long, 1.2 m wide and 0.3 m high. The glass canopy protects the internal components from wind, dust and water. Fig. 2(a) and (b) shows a schematic of the LMC. Fig. 2(c) is the cross-sectional view showing ray tracing conducted for the LMC under normal angle of incidence on the box. This concentrator has been optimised for high temperature (100–220 °C) thermal applications and has been recently retrofitted for combined heat and power generation by installing highly efficient silicon cells coupled to a cooling channel [25,26].

The LMC provides the hybrid receiver with concentrated radiation and the hybrid receiver transforms it into useful electrical and thermal energy. To estimate the overall performance of the system, the whole configuration has been analysed as an integrated package.

The orientation of the LMC, sun angle, shadows from the structure on the mirrors, and the geometrical arrangement of the mirrors can affect the spatial and angular distribution of light at

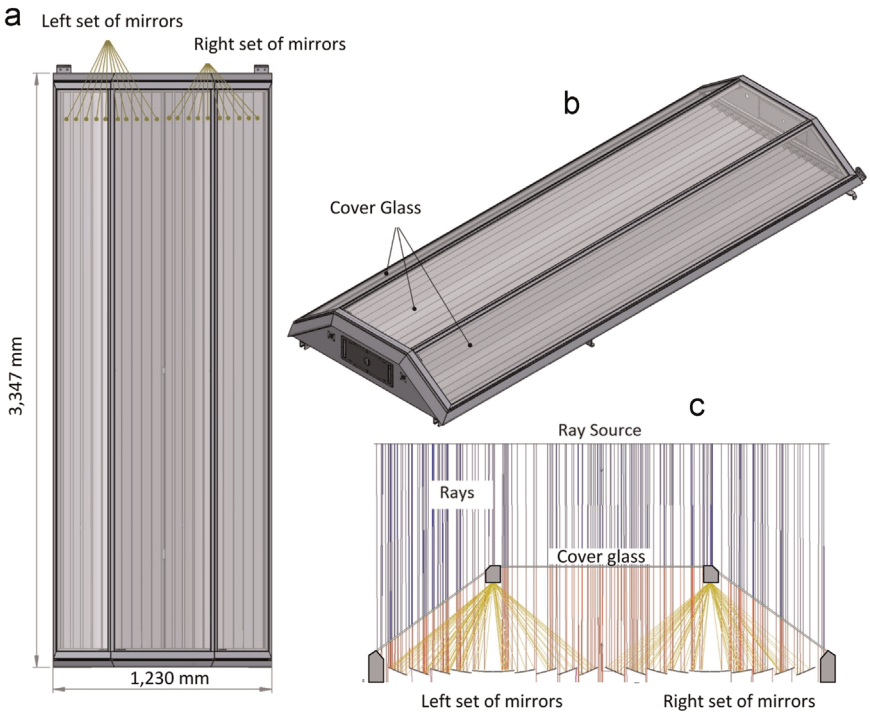

Fig. 2. Schematic of the LMC developed by Chromasun Pty Ltd: (a) top view of the LMC, (b) isometric view of the LMC, and (c) cross section of the LMC, consisting of 2 sets of narrow curved mirrors focusing sunlight onto two focal lines.

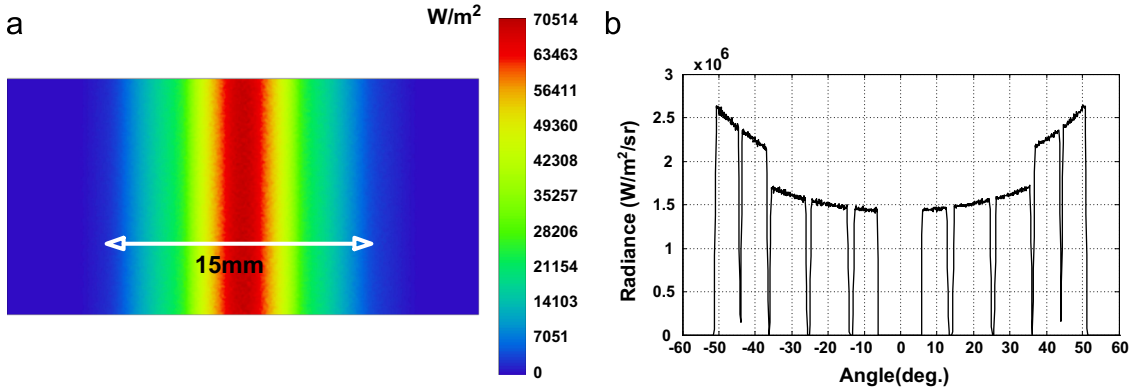

Fig. 3. Flux distribution at the bottom face of front glass of the LMC: (a) spatial distribution of irradiance (W/m^2); the width of the spot size is 15 mm containing more than 99% of incoming radiation and (b) angular distribution of the radiance ($W/m^2/sr$).

the focal region. In addition to this, the spectral distribution of the sunlight at the focal region of the LMC is different from the original solar spectrum because the sunlight passes through the cover glass and gets reflected by the dichroic mirror before reaching the receiver; both of these components have wavelength dependent optical properties (reflectivity and transmissivity).

3.2. Optical modelling of the LMC

Since the LMC has a relatively complicated concentrating mechanism including a set of small mirrors with different curvatures and complicated shadowing effects, computer aided ray tracing is required. In this study ZEMAX (version 13) [27] software was chosen to study the optical characteristics of the system. To do this, the sun was defined as a radial source at infinity. Since the sun is not a point source (because of its significant size compared to its distance from the earth), a sun half angle of 0.27° [11] was incorporated in the model. Accounting for this is important because it can influence the radiation distribution at the focal region of solar concentrators.

In a spectrally splitting receiver, the variation of the spectrum at the focal region plays a key role in determining the system performance. Because the LMC uses Fresnel reflectors to concentrate the light, very little of the diffuse portion of the global radiation reaches the receiver(s). Hence only the spectrum of beam radiation was defined as the ray source in ZEMAX. This data was acquired from the reference air mass 1.5 solar spectrum [28]. Total solar radiation flux is calculated using the data provided by [28] as $I = \int_{280\ \mathrm{nm}}^{4000\ \mathrm{nm}} I_\lambda\ \mathrm{d}\lambda$, where I is the irradiance of the light source (W/m^2), I_λ is the direct and circumsolar spectral irradiance of the sunlight, acquired from [28], and λ is the wavelength. The above integration was carried out numerically resulting in 900 W/m^2 as the source power.

3.3. The spatial and angular flux distribution on the receiver

Fig. 3 shows the distribution of the incoming power on the bottom face of the front glass (e.g. the aperture area of the hybrid receiver). In this figure it has been assumed that the tracking system and the surface quality of the mirrors are ideal; any variation in these factors can change the spatial distribution of the flux at the focal point of any solar concentrator. For example, including tracking errors and mirror surface inaccuracies in the optical modelling will cause a wider focal spot (lower solar concentration) as well as a non-symmetrical flux distribution.

Fig. 3b shows the angular distribution of the incoming flux on the bottom surface of the front glass. This parameter is important in designing the side absorber walls as well as the dichroic coating since this design relies on not having the side walls intercept the rays before they reach the dichroic coating. At the same time, the dichroic coating should be designed based on the weighted mean angle of incidence to optimise the optical performance of the coating that depends on the angle of incidence [29]. By changing the angle of incidence on thin film interference coatings, the reflection transmission curve deviates from the design point [12].

3.4. The weighted mean angle of incidence on the dichroic filter

In the proposed geometry, the thin film coating (dichroic filter) should be designed for non-collimated, concentrated radiation, as shown in Fig. 3b. Since the reflection–transmission characteristics of thin film optical filters are sensitive to the incident angle, different approaches such as curved [11] and tapered filters [29] have been suggested. Because these methods require sophisticated fabrication processes, a flat filter was considered here but the effect of incident angle was minimised by optimising the filter for the power weighted mean angle of incidence (*PWMAI*).

The total radiative power (W) to the surface of the dichroic coating is given by [30]

$$I(W) = \int_A \int_{2\pi} \int_0^{\infty} I(r, \hat{s}, \lambda)\hat{n}\cdot\hat{s}\ \mathrm{d}\lambda\ \mathrm{d}\Omega\ \mathrm{d}A. \tag{1}$$

where $I(r, \hat{s}, \lambda)$ is the spectral directional radiation intensity (W/m^2/nm/sr) at a location specified by the position vector of r; $\hat{n}$ is the unit normal vector of the receiving surface, $\hat{s}$ is the unit vector in the direction of the incoming radiation towards the surface, λ is the wavelength (nm), Ω is the solid angle, and A is the surface area of the receiver. For a flat surface depicted in Fig. 4, $\hat{n}$ is a unit vector in the Y direction and $\hat{n}\cdot\hat{s}$ describes the cosine effect of the angle of incidence ($\cos\theta$). Noting that $\mathrm{d}\Omega = \sin(\theta)\ \mathrm{d}\theta\ \mathrm{d}\phi$, Eq. (1) can be described in spherical coordinates to simplify the calculations as shown in Eq. (2). The coordinate system is defined (with respect to the receiver) in Fig. 4:

$$I(W) = \int_A \int_0^{2\pi} \int_0^{\frac{\pi}{2}} \int_0^{\infty} I(r, \theta, \phi, \lambda)\cos(\theta)\sin(\theta)\ \mathrm{d}\lambda\ \mathrm{d}\theta\ \mathrm{d}\phi\ \mathrm{d}A. \tag{2}$$

The spectral and spatial integration was carried out based on the ray tracing results. The radiant intensity $I(\theta, \phi)$ (in W/sr) is calculated by ZEMAX, which includes the cosine effect. Hence Eq. (2) can be simplified as

$$I(W) = \int_{2\pi} I(\theta, \phi)\sin(\theta)\ \mathrm{d}\theta\ \mathrm{d}\phi. \tag{3}$$

Since the absolute value of θ drives the optical properties of the dichroic coating, the PWMAI was calculated for half of the incident flux (symmetric about the $Y-Z$ plane). It will be shown that this minimises the standard deviation of the angle of incidence (SDAI) on the dichroic coating. In this modelling, the sun has been assumed to be normal to the collector box hence there is no longitudinal or transversal angle of incidence on the collector box. Since the concentrating mirrors have a cylindrical shape, they create an angular distribution only in the $X-Y$ plane.

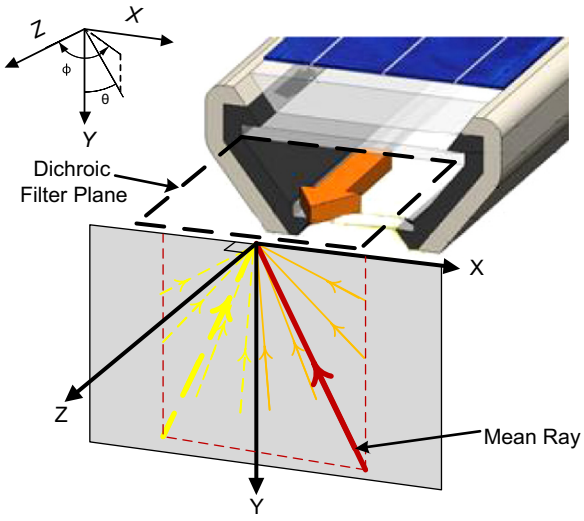

Fig. 4. Spherical coordinate system at the location of the thin film filter; The Z-axis is along the length of the collector; the Y-axis is normal to the dichroic surface; all the rays are in the X–Y plane. The mean ray, depicted by a solid bold arrow (red and yellow) is the power weighted mean average of the rays impinging upon the dichroic filter. The red and yellow arrows correspond to the mean ray for the set of the incoming rays either side of the Y–Z symmetry plane. (For interpretation of the references to colour in this figure caption, the reader is referred to the web version of this paper.)

The PWMAI and SDAI of the angle of incidence on the thin film coating can be calculated using

$$\theta_{mean} = \frac{\int_0^{\pi}\int_0^{\pi/2} \theta I(\theta, \phi)\sin(\theta)\ \mathrm{d}\theta\ \mathrm{d}\phi}{\int_0^{\pi}\int_0^{\pi/2} I(\theta, \phi)\sin(\theta)\ \mathrm{d}\theta\ \mathrm{d}\phi}, \tag{4}$$

$$\sigma = \sqrt{\frac{\int_0^{\pi}\int_0^{\pi/2} (\theta - \theta_{mean})^2 I(\theta, \phi)\sin(\theta)\ \mathrm{d}\theta\ \mathrm{d}\phi}{\int_0^{\pi}\int_0^{\pi/2} I(\theta, \phi)\sin(\theta)\ \mathrm{d}\theta\ \mathrm{d}\phi}}, \tag{5}$$

where θ_{mean} and σ are PWMAI and SDAI, respectively. Using the above equations we end up with $\theta_{mean} = 18.6°$ and $\sigma = 4°$. If normal AOI instead of the calculated PWMAI had been used, the standard deviation, σ, would have increased from 4° to 10°. This shows that using θ_{mean} will result in a narrower angle of incidence distribution and more accurate light filtering by the dichroic coating.

3.5. Thin film optical filter design and fabrication

The dichroic filter is a long pass filter with cut-off wavelength at about 600 nm and should be optimised for the PWMAI (18.6°) calculated in the previous section. TiO_2 and SiO_2 were selected as the high and low refractive index materials, respectively. For this pair of materials, use of a ($0.5H\ L\ 0.5H$) configuration results in a satisfactory performance as a long pass filter on glass substrate [17], where H and L are quarter wavelength thicknesses of TiO_2 and SiO_2, respectively, at a reference wavelength.

Because the refractive indices of these materials depend on the coating process and their crystal structure, a thin layer of each material was deposited on a silicon wafer using electron beam evaporation employing an Intlvac Nanochrome Electron Beam Evaporation system at low substrate temperature in the range of 27–60 °C. The refractive indices of these layers were then

measured using ellipsometry, with the results presented in Fig. 5. The growth rates of SiO_2 and TiO_2 were 1 Å/s and 0.5 Å/s, respectively.

Designing a simple filter with low stack thickness improves its cost effectiveness as well as its endurance under thermal cycling. Hence, we started the filter design with an initial 7 layer-stack formula of $(0.5H\ L\ 0.5H)^3$. The reference wavelength was 500 nm and the refractive indices acquired above were used in the design process. The front and back media were glass and air, respectively. The layers were then refined to match a transmission target. The refinement process was carried out in Openfilters [31], an open source code for designing wave interference filters. The mathematical procedure of the code has been explained in [32].

In the refined stack, all layers thinner than 10 nm have been eliminated. However this refinement was processed based on an ideal edge filter target, as depicted by the dashed line in Fig. 6(a), regardless of the solar spectrum. The result is not necessarily the optimum filter because the solar spectrum has not been accounted for. Through a second optimisation stage, the filter minima location can be optimised according to the solar spectrum. In this study, this task has been accomplished by a simple optimisation process of the electrical output of the PV cells over the spectral distribution of the transmitted light through the filter.

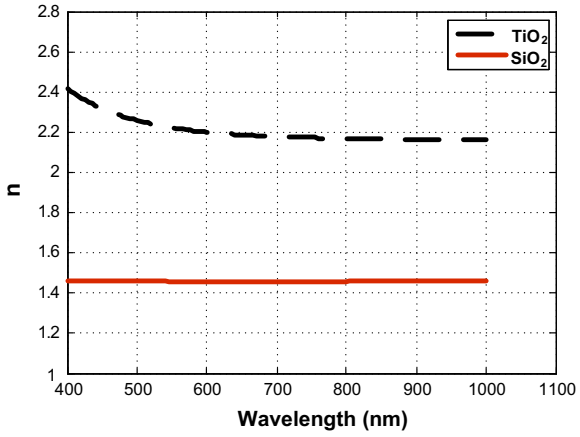

Fig. 5. Measured refractive indices of TiO_2 and SiO_2 deposited by e-beam evaporation at low substrate temperature.

The equations for calculating the spectral transmission and reflectance of a thin film structure are well known [17]. Here, we show the application of them in optimising the minima loci of the transmission curve according to the solar spectrum and spectral response of the cells. For this purpose the open circuit voltage, V_{OC}, and fill factor, FF, were considered 0.645 and 0.776, respectively, at 25 °C which are in the typical range of the cells as reported in [33]. The efficiency of the cell for the spectral band corresponding to the filter in the effective spectral band of the filter, i.e. 300–1200 nm, can be approximated as below:

$$\eta_{pv} = \frac{\mathrm{FF}\, V_{OC} \int_{300}^{1200} \mathrm{SR}\, I_\lambda^T \,\mathrm{d}\lambda}{\int_{300}^{1200} I_\lambda^T \,\mathrm{d}\lambda}, \tag{6}$$

where I_λ^T and SR are the spectral irradiance of the transmitted radiation and the spectral response of the cell, respectively. I_λ^T is calculated as $I_\lambda^T = T_\lambda\ I_\lambda$, where T_λ is the spectral transmissivity of the thin film assembly and can be calculated as [17]

$$T_\lambda = \frac{4\eta_0\, Re(\eta_m)}{(\eta_0 B + C)(\eta_0 B + C)^*}, \tag{7}$$

where admittance, η, is calculated as $\eta_p = N\xi/\cos(\nu)$ for p-polarisation and $\eta_s = N\xi\cos(\nu)$ for s-polarisation. N is the complex refractive index as $n - ik$ and $\xi = 2.6544 \times 10^{-3}$ s. η_0 and η_m are the admittance of air and substrate, respectively. B and C can be calculated as [17]

$$\begin{bmatrix} B \\ C \end{bmatrix} = \prod_{r=1}^{q} \begin{bmatrix} \cos(\delta_r) & i\sin(\delta_r)/\eta_r \\ i\eta_r \sin(\delta_r) & \cos(\delta_r) \end{bmatrix} \times \begin{bmatrix} 1 \\ \eta_m \end{bmatrix}, \tag{8}$$

where $\delta_r = 2\pi N s d_r \cos(\nu)/\lambda$. The parameter d represents the physical thickness of the rth layer, while ν is the angle of the ray in the film, derived from Snell's law.

In order to move the minima of the transmission curve, the thickness of the layers is multiplied by the same scalar factor, s, to make all layers consistently thicker or thinner. For $s < 1$ and $s > 1$ the transmission curve is shifted towards short and long wavelengths, respectively. By maximising η_{pv} in Eq. (6) over the transmitted spectrum, the optimum filter design and layer thicknesses can be determined.

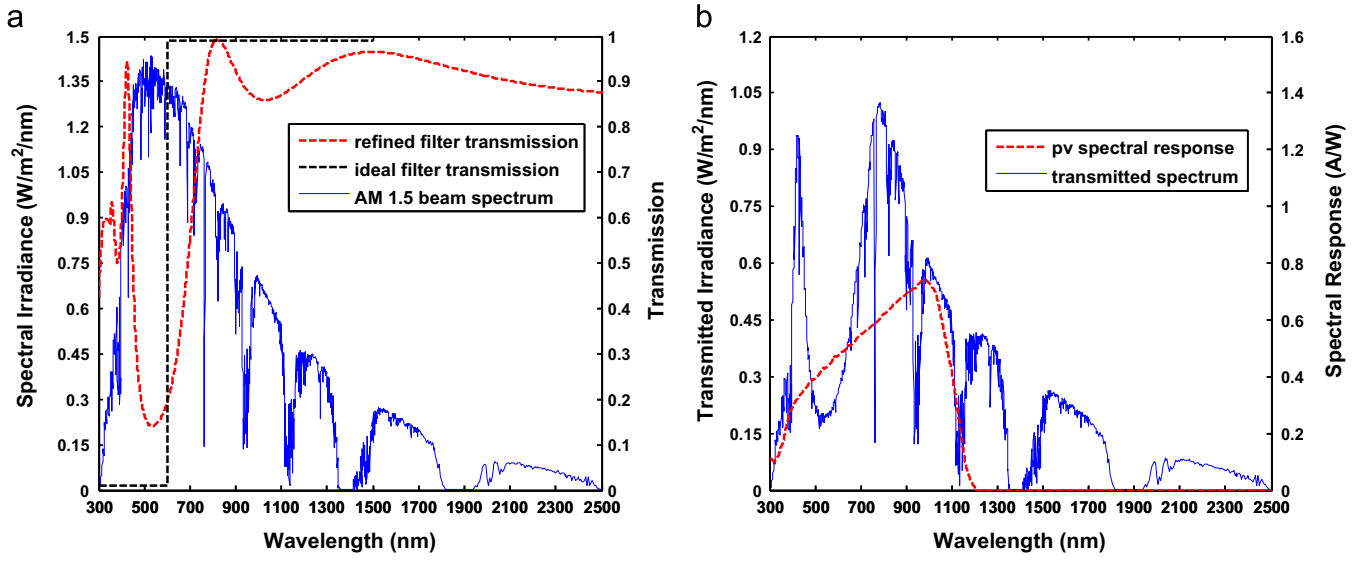

Fig. 6. (a) Spectral transmission of the thin film filter vs. the direct beam component of the AM 1.5 solar spectrum and (b) spectrum of the transmitted radiation through the thin film filter vs. the spectral response of the high efficiency Si solar cell.

3.6. Optical properties of the heat transfer liquids

As mentioned before, three different types of heat transfer liquid were considered for absorbing the IR range of the spectrum. Fig. 7 presents their absorption indices. The transmission values in Fig. 7 have been calculated using Beer's law: $T = e^{(-4\pi kd)/\lambda}$, where T is the transmission, k is the absorption index, d is the light path-length, and λ is the wavelength.

4. Results and discussion

The optimisation of the filter started with the refined stack and ended up with the optimal stack as presented in Table 1. Fig. 8a shows the variation of η_{pv} as a function of s. In this figure, a value of 0.84 for the scalar factor s corresponds to the maximum PV conversion efficiency of approximately 27%, i.e. the optimal stack. It is important to note that this efficiency was calculated based on the transmitted power through the filter as described in Eq. (6).

Fig. 8b shows the effect of s on the transmission curves; the optimal and refined stacks transmission curves have been denoted by $s=0.84$ and $s=1$, respectively. The minimum transmission of the optimal stack occurs at 460 nm at 18° AOI.

The fabricated filter transmission curve is presented in Fig. 10a. The measurement results were compared for AOI=0° for both cases. The designed 5-layer filter corresponds to the result of the simulation, and the fabricated 5-layer filter corresponds to the result of the optical transmission measurements on the fabricated filter. A very close match is observed between the curves. There is a divergence for wavelengths of shorter than 400 nm which is caused by the absorption of TiO_2. In the simulated model, TiO_2 was considered non-absorbing for all wavelengths. However this discrepancy is useful as the short wavelengths are blocked. These two curves are compared against an ideal sharp edge long pass filter that cannot be generally achieved by configurations with small number of layers.

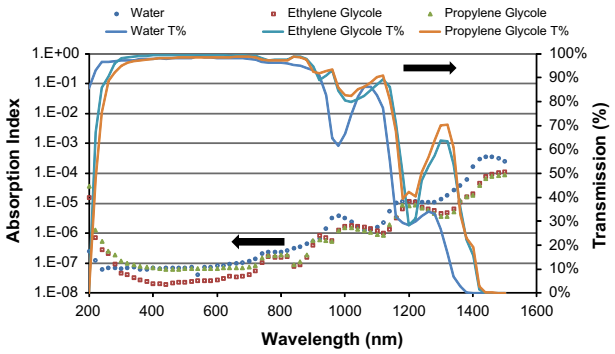

Fig. 7. Measured absorptive index of water [34], ethylene glycol, and propylene glycol [20] accompanied with the respective transmission coefficient.

Table 1
Structure of the dichroic coating for fabrication.

Refined stack			Optimal stack	
#	Material	Thickness (nm)	Material	Thickness (nm)
1	TiO_2	55	TiO_2	46
2	SiO_2	94	SiO_2	79
3	TiO_2	64	TiO_2	54
4	SiO_2	96	SiO_2	81
5	TiO_2	50	TiO_2	42
	Total	359	Total	302

The long pass filter of Fig. 10a was assembled in the proposed receiver configuration to function as a band pass filter. The test assembly is shown in Fig. 9. The liquid in this measurement was water, which has good optical and heat transfer properties. The optical transmission of the whole assembly, the receiver, is presented in Fig. 10b against the spectrum of AM1.5 and an ideal sharp band pass filter with the cut-off edges at 600 nm and 1125 nm. 1125 nm has been chosen according to the band gap of silicon. The short side of the band can be tuned according to the heat-electricity demand ratio. That is, by moving the short edge towards shorter wavelength the heat to electricity production ratio decreases and vice versa. Thus, tunability can be achieved by scaling the thickness of the layers in the thin film structure.

The transmitted and blocked spectra based on the transmission curve of Fig. 10b are presented in Fig. 10c. The transmitted radiation reaches the PV cells and the blocked radiation is either absorbed directly by water or is reflected towards, and absorbed by, the side walls and then transferred into water as heat.

The baseline efficiency of the Si cells considered in this paper is about 20.6% at 25 °C and a CR of 1 under the full AM1.5 spectrum. However they can convert 26.1% of the transmitted radiation from this filter to electricity. The total PV conversion of the whole system based on the total power reaching the front glass decreases to 12.9% because less light is directed to the cells. It should be noted that these PV conversion values are functions of cell temperature.

The authors have shown that employing spectral splitting reduces the heat load on the PV cells, which helps us to keep the solar cells at lower temperature under concentrated radiation than for cells exposed to full spectrum solar radiation [35]. It was demonstrated that at a CR of 20, the cell temperature can increase by 15 °C above the heat sink temperature. With such an increase in the cell temperature, the efficiency of the PV cells can drop by about 1% in absolute value.

The blocked radiative power is converted into heat in the thermal receiver which is now thermally decoupled from the cells and can reach temperatures above the working limit temperature of the cells. The heat transfer characteristics of beam splitting receivers with similar geometry have been studied extensively by the authors [36] showing that the cell temperature increases by approximately 1 °C per 8 °C rise in the temperature of the thermal receiver.

The sensitivity of the filtering system to the AOI in the short wavelengths, where the thin film structure is driving the optics, is presented in Fig. 10d. By increasing the AOI the transmission curve of the whole receiver shifts towards shorter wavelengths. The minima of the transmission curve move from 480 nm to 453 nm when the AOI on the front glass changes from 0° to 40°. Slightly more variation is observed in the midpoint of the cut-off edge where the transmission of the filter is 50%. The 50% transmission point moves from 598 nm at AOI=0° to 550 nm at AOI=40°.

For a more detailed analysis of the receiver optical performance, ray tracing modelling based on the fabricated filter was carried out in ZEMAX. Fig. 11a shows the light propagating in the hybrid receiver. As it is seen in this figure, the highest level of concentration is at the front glass. A part of the incoming radiation is reflected by the rear glass with the dichroic coating at its top face (far from the liquid). The majority of the reflected light is absorbed by the side walls however 3.9% of that bounces back out of the receiver through the front glass, which combines with 4.3% Fresnel reflection of the front glass–air interface. As it is shown in Table 3, the total reflection loss of the receiver is 8.2%. As has been mentioned before, a part of the radiation is absorbed directly by water. Fig. 11b shows the absorbed power (in Watts) by water in a 40 mm long section. Since water is highly absorbing in the infrared, the majority of absorption takes place in the liquid channel just on top of the front glass. However, in the 1100–1400 nm band,

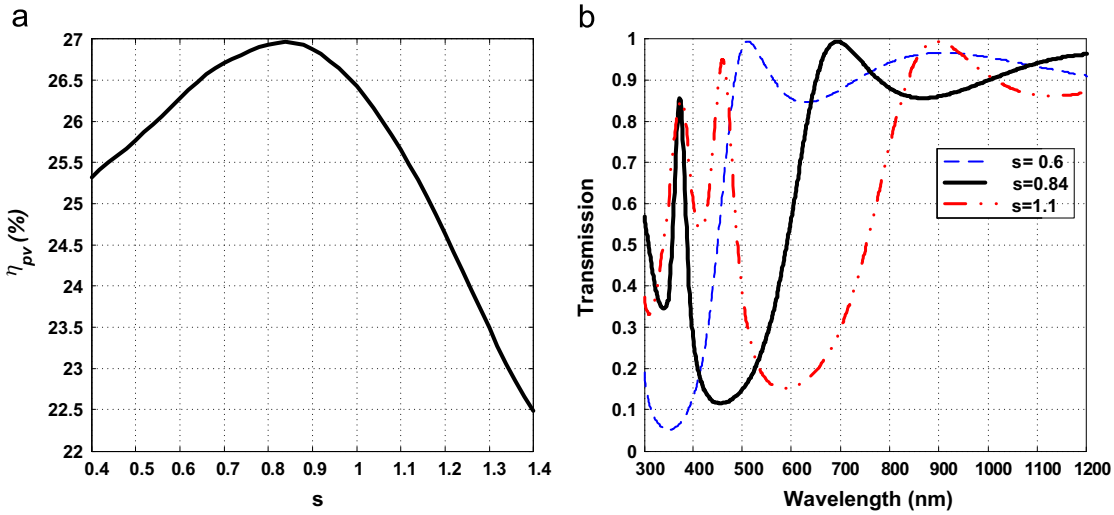

Fig. 8. (a) Effect of s on the efficiency of the silicon cells; the efficiency is based on the transmitted light in the range of 300–1200 nm and (b) the effect of s on the transmission curve of the filter; $s=0.84$ corresponds to the optimum filter with the maximum PV conversion efficiency at 18° AOI.

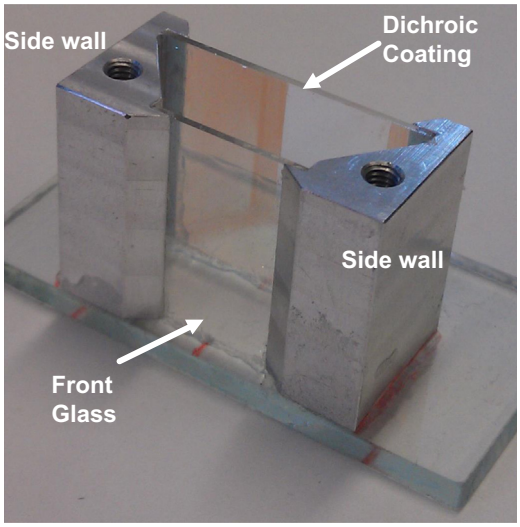

Fig. 9. The test sample of the receiver for measuring its optical transmission.

water has moderate absorption and light rays in this range which penetrate deeper into water and are absorbed in deeper regions. It should be noted that in this work, pure water was considered for the volumetric absorption and its scattering effect was ignored.

The graph in Fig. 12 shows the spectral distribution of different components of radiation in the fabricated receiver. It should be remembered that the aim of the design was to direct the wavelength between 600 nm and 1125 nm to silicon cells; Fig. 12c shows that the majority of the radiation reaching the PV is in this spectral band. On the other hand the absorbing side walls absorb the radiation below 600 nm that is reflected by the dichroic coating, as seen in Fig. 12d. The missed reflected rays in Fig. 12(b) contain wavelengths across the whole solar spectrum range because a portion of this flux is due to Fresnel reflection from the front glass that causes reflection across whole the spectrum hitting the glass; however another component of the reflected-missed rays comprises the wavelengths reflected by the dichroic coating and missed by the side walls . These wavelengths are mainly in 300–600 nm range. This is the main reason why the graph in Fig. 12b has much higher intensity in this range.

The results of numerical integration of the spectral distribution on the PV cells are shown in Table 2. It should be noted that in this table the percentage is based on the total amount of energy reaching the PV cells. The ideal percentage assumes an ideal band pass filter with sharp cut-off wavelengths at 600 nm and 1125 nm without any optical losses. Such an ideal filter is 100% transparent within this range and 100% reflective outside it.

The energy absorbed by each component of the receiver was calculated by integrating the respective flux distribution impinging upon each part. Table 3 presents the energy balance of the model. The percentage is based on the total energy entering the receiver at the front glass. It should be noted that the reflection losses include the Fresnel reflection from the front glass and the light reflected back out of the receiver by the dichroic coating.

The analysis shows that by using the current receiver geometry, 54.5% of the radiation hitting the front glass reaches the cells, with 73.3% of this flux within the desired wavelength range. This is comparable to the ideal case in which the power of the AM1.5 spectrum in 600–1125 nm range reaches the cell. For the ideal case, 48.7% of the total AM1.5 power would have been directed to the cells and 100% of that would have been in the desired range. Two causes for this difference are (1) non-ideal spectral splitting and (2) reflection losses. Non-ideal filtering can be improved by designing a sharper dichroic filter with more layers at the cost of higher fabrication expense. The reflection losses can also be mitigated by optimising the geometry of the dichroic coating, e.g. using a V-shape dichroic filter to direct the rays towards the side walls more effectively. The Fresnel losses from the front glass can be reduced by the use of antireflection coatings.

Unlike the PV efficiency, the efficiency of the thermal component of the system is less sensitive to the performance of the dichroic mirror because the absorbing side walls of the receiver can absorb all the wavelengths across the solar spectrum efficiently. In order to verify the worthiness of such a filtering device from an efficiency point of view, the PV conversion efficiency with the measured filter, ideal filter, and without any filtering has been presented in Table 4.

Here, “no filtering” refers to the conversion efficiency of the cells under the full spectrum without any optical losses which occur due to the presence of the filter. Using the “ideal filer” reduces the total PV conversion of the system to 14.5% based on the total power reaching the hybrid receiver; again, this represents the case with no optical losses. The “fabricated filter” takes the optical losses and non-ideal spectral splitting effects into account. Compared to ideal filtering, the total PV conversion and the conversion based on the band of the light reaching the cells are 1.9% and 3.7% lower (in absolute values), respectively. It is well known that the thermal and electrical efficiencies of hybrid solar

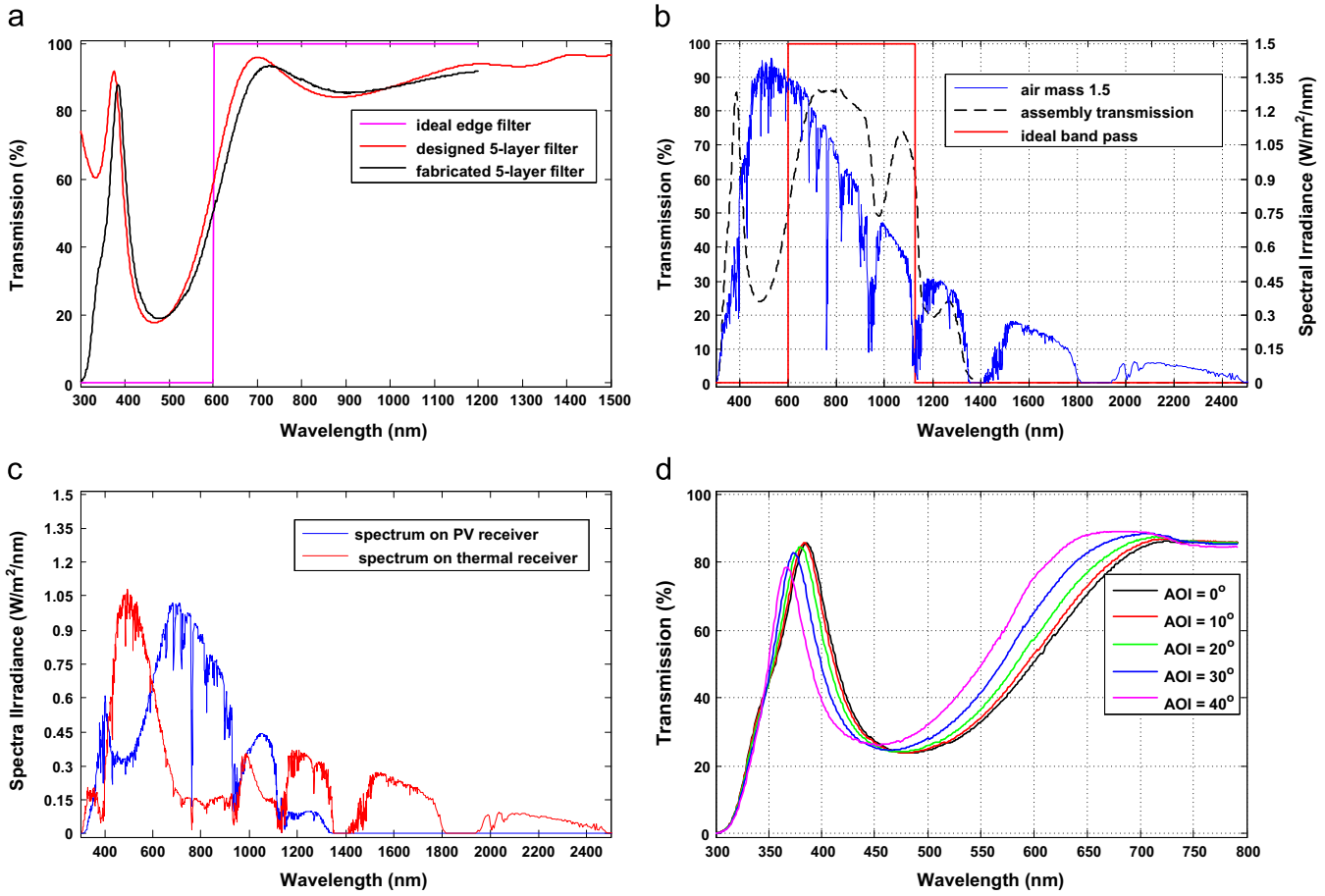

Fig. 10. The measurement results for the receiver sample: (a) the ideal edge filter is considered a sharp long pass filter with cut-off wavelength at 600 nm, (b) the transmission of the receiver sample including the thin film filter and water as the liquid filter; the ideal band pass filter has cut-off edges at 600 nm and 1125 nm for Si cells, (c) the comparison between the spectral distribution of the radiation reaching the PV and thermal modules independently, and (d) the effect of the angle of incidence on the front glass of the receiver.

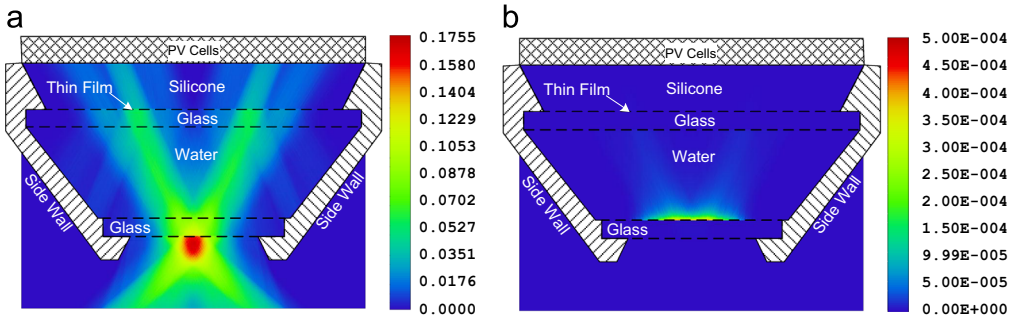

Fig. 11. Ray tracing simulation of the hybrid receiver: (a) the incident flux at each point in the receiver and (b) the absorbed flux inside the water volume. The values reported on the colour bars are in Watts showing the amount of power at each point for 40 mm of the receiver length. (For interpretation of the references to colour in this figure caption, the reader is referred to the web version of this paper.)

collectors are typically lower than those of separate thermal and photovoltaic collectors, respectively, which is the case here as well.

The solar weighted transmission of the filter accompanied by the transmission values for the liquid channel including the water layer, front and rear glass panels are presented in Table 5. As it is observed in this table, the dichroic filter is highly reflective in the spectral band shorter than 600 nm and is highly transparent in the desired band between 600 nm and 1125 nm. The high transmission of the dichroic filter (92.6%) beyond 1125 nm is not an issue as long as the transmission of the liquid channel in the same range is low; the liquid channel has 12.5% transmission in this range. This value is determined by the intrinsic absorption coefficient of the liquid and its thickness.

Increasing liquid thickness can suppress the transmission above 1125 nm but it should be noted that it can reduce the transmission in 600–1125 nm range as well. Lower transmission in this range means lower electrical power. So we can optimise the thickness of the liquid layer in accordance to the desired ratio of electrical to thermal output. Another possible solution for optimising the transmission of the liquid channel at 1125 nm is using other liquids with a better

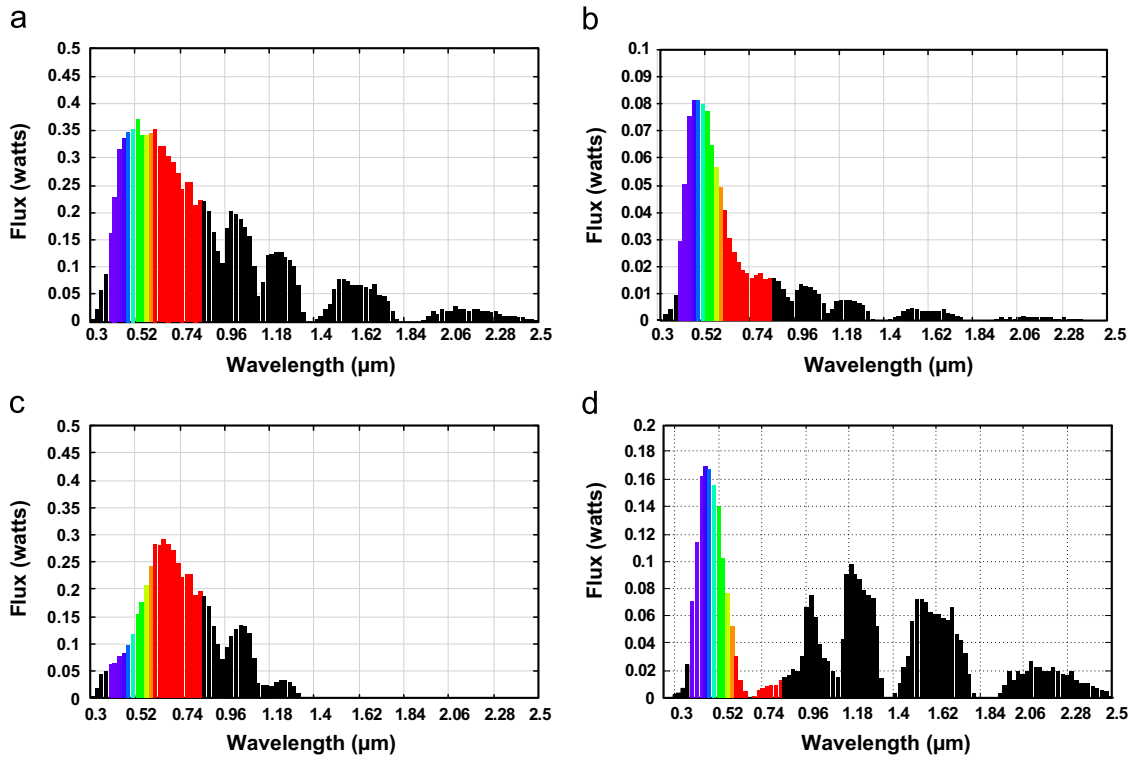

Fig. 12. The spectral distribution of the (a) incoming flux, (b) reflected missed flux, (c) absorbed flux by the cells, and (d) the radiation absorbed by the thermal components; the vertical axis is in Watts.

Table 2
Spectral analysis of the radiation reaching the PV cells.

Spectral band	Percentage	Ideal percentage	Comment
$\lambda < 600$ nm	22.6	0	Undesirable range
600 nm $<\lambda<$ 1125 nm	73.3	100	Desirable range
$\lambda >$ 1125 nm	4.1	0	Undesirable range

Table 3
Energy balance of the model; percentage of the energy absorbed by each part of the hybrid receiver with respect to the total energy of light impinging upon the front glass.

Items	Percentage
Absorbed by the front glass	0
Absorbed by water	22.9
Absorbed by the rear glass	0.00
Absorbed by the side walls	14.3
Absorbed by the PV cells	54.5
Total reflection loss (inc. Fresnel and missed rays)	8.2

Table 4
PV conversion performance under different conditions and spectral bands.

PV operation condition	η_{PV} based on total incoming power (%)	η_{PV} based on power reaching the cells (%)
No filtering	20.6	20.6
Ideal filter	14.5	29.8
Fabricated filter	12.6	26.1

matched spectral absorption index. This will be covered in the future work.

As previously mentioned the Fresnel reflection loss from the front glass was 4.3%. This loss occurs mainly due to the reflection from the front face of the glass panel, as the back face is in direct contact with water (smaller difference in refractive index $n=1.33$ for water, $n=1.5$ for K10 glass). The other source of reflection loss is the reflected rays from the dichroic coating that miss the receiver side walls. These rays leave the receiver cavity through the front glass. This issue can be addressed by further optimising the geometry of the receiver, e.g. using a V-shape rear glass to slightly tilt the dichroic mirror and direct the reflected light towards the side absorbers more efficiently. Using this method, one should be careful about the effect of angle of incidence on dichroic coatings i.e. the dichroic coating should be optimised for the new angular distribution of light that includes the tilt angle of the mirror.

Table 5
Transmission of the dichroic filter and the liquid channel.

Optical medium	Spectral band (nm)	Transmission (%)
Dichroic filter	300–600	33
	600–1125	72
	1125–4000	92.6
Liquid channel	300–600	98.2
	600–1125	91.7
	1125–4000	12.5

5. Conclusion

This paper has presented the possibility of combining dichroic filters with direct absorbing liquids to achieve efficient spectral splitting of sunlight in a hybrid solar receiver. The receiver geometry was optimised for Chromasun's linear micro-concentrator; however it can be optimised for other types of concentrators with different sizes, such as parabolic troughs. The modelling results showed that the receiver is capable of directing 54.5% of the solar spectrum to the PV cells; 73.3% of this energy is in the desired

range of 600–1125 nm band. The vast majority of the remaining solar spectrum is absorbed by the liquid channel and is converted to heat. Using this spectral splitting technique, the temperature of the thermal part of the receiver has been decoupled from the PV cell, such that the maximum temperature of the thermal absorber is not limited by the cell operating temperature.

Acknowledgements

This work was performed in part at the Melbourne Centre for Nanofabrication (MCN) in the Victorian Node of the Australian National Fabrication Facility (ANFF). The authors would also like to thank the Australian Renewable Energy Agency (ARENA) for funding A. Mojiri and this research (Grant Ref.: s-2006-ASI).

References

[1] A. Royne, C.J. Dey, D.R. Mills, Cooling of photovoltaic cells under concentrated illumination: a critical review, Sol. Energy Mater. Sol. Cells 86 (4) (2005) 451–483.
[2] H. Cotal, C. Fetzer, J. Boisvert, G. Kinsey, R. King, P. Hebert, H. Yoon, N. Karam, III–V Multijunction solar cells for concentrating photovoltaics, Energy Environ. Sci. 2 (2) (2009) 174–192.
[3] A. Imenes, D. Mills, Spectral beam splitting technology for increased conversion efficiency in solar concentrating systems: a review, Sol. Energy Mater. Sol. Cells 84 (1) (2004) 19–69.
[4] A. Mojiri, R. Taylor, E. Thomsen, G. Rosengarten, Spectral beam splitting for efficient conversion of solar energy review, Renew. Sustain. Energy Rev. 28 (2013) 654–663.
[5] A. Barnett, C. Honsberg, D. Kirkpatrick, S. Kurtz, D. Moore, D. Salzman, R. Schwartz, J. Gray, S. Bowden, K. Goossen, et al., 50% Efficient solar cell architectures and designs, in: Conference Record of the 2006 IEEE Fourth World Conference on Photovoltaic Energy Conversion, vol. 2, IEEE, 2006, pp. 2560–2564, http://dx.doi.org/10.1109/WCPEC.2006.279768.
[6] F. Crisostomo, R.A. Taylor, A. Mojiri, E.R. Hawkes, D. Surjadi, G. Rosengarten, Beam splitting system for the development of a concentrating linear Fresnel solar hybrid PV/T collector, in: ASME 2013 Heat Transfer Summer Conference Collocated with the ASME 2013 Seventh International Conference on Energy Sustainability and the ASME 2013 11th International Conference on Fuel Cell Science, Engineering and Technology, American Society of Mechanical Engineers, 2013, pp. V001T01A029–V001T01A029, http://dx.doi.org/10.1115/HT2013-17221.
[7] A. Barnett, X. Wang, High efficiency, spectrum splitting solar cell assemblies: Design, measurement and analysis, in: Optics for Solar Energy, Optical Society of America, 2010, p. SWB1, http://dx.doi.org/10.1364/OSE.2010.SWB1.
[8] V. Khvostikov, A. Vlasov, S. Sorokina, N. Potapovich, N.K. Timoshina, M. Shvarts, V. Andreev, High-efficiency (η=39.6%, AM 1.5 D cascade of photoconverters in solar splitting systems, Semiconductors 45 (6) (2011) 792–797.
[9] M. Chendo, M. Jacobson, D. Osborn, Liquid and thin-film filters for hybrid solar energy conversion systems, Sol. Wind Technol. 4 (2) (1987) 131–138.
[10] M.A. Hamdy, F. Luttmann, D. Osborn, Model of a spectrally selective decoupled photovoltaic/thermal concentrating system, Appl. Energy 30 (3) (1988) 209–225.
[11] S. Jiang, P. Hu, S. Mo, Z. Chen, Optical modeling for a two-stage parabolic trough concentrating photovoltaic/thermal system using spectral beam splitting technology, Sol. Energy Mater. Sol. Cells 94 (10) (2010) 1686–1696.
[12] M. Peters, J.C. Goldschmidt, P. Löper, B. Groß, J. Üpping, F. Dimroth, R.B. Wehrspohn, B. Bläsi, Spectrally-selective photonic structures for PV applications, Energies 3 (2) (2010) 171–193.
[13] F. Crisostomo, R.A. Taylor, T. Zhang, I. Perez-Wurfl, G. Rosengarten, V. Everett, E.R. Hawkes, Experimental testing of SiN_x/SiO_2 thin film filters for a concentrating solar hybrid PV/T collector, Renewable Energy 72 (2014) 79–87.
[14] M. Vivar, V. Everett, A review of optical and thermal transfer fluids used for optical adaptation or beam-splitting in concentrating solar systems, Progress in Photovoltaics: Research and Applications 22 (6) (2014) 612–633.
[15] R. Taylor, S. Coulombe, T. Otanicar, P. Phelan, A. Gunawan, W. Lv, G. Rosengarten, R. Prasher, H. Tyagi, Small particles, big impacts: a review of the diverse applications of nanofluids, J. Appl. Phys. 113 (1) (2013) 011301.
[16] R.A. Taylor, T.P. Otanicar, Y. Herukerrupu, F. Bremond, G. Rosengarten, E. R. Hawkes, X. Jiang, S. Coulombe, Feasibility of nanofluid-based optical filters, Appl. Opt. 52 (7) (2013) 1413–1422.
[17] H. Macleod, Thin-Film Optical Filters, Series in Optics and Optoelectronics, 4th edition,. Taylor & Francis, Boca Raton, Florida, U.S, 2010.
[18] J.E. Minardi, H.N. Chuang, Performance of a black liquid flat-plate solar collector, Sol. Energy 17 (3) (1975) 179–183.
[19] T.P. Otanicar, P.E. Phelan, R.S. Prasher, G. Rosengarten, R.A. Taylor, Nanofluid-based direct absorption solar collector, J. Renew. Sustain. Energy 2 (3) (2010) 033102.
[20] T.P. Otanicar, P.E. Phelan, J.S. Golden, Optical properties of liquids for direct absorption solar thermal energy systems, Sol. Energy 83 (7) (2009) 969–977.
[21] V. Everett, A. Blakers, J. Cotsell, J. Harvey, R. van Scheppingen, D. Walters, Improving the efficiency of linear concentrator receiver systems, in: Solar09, the 47th ANZSES Annual Conference, Townsville, 2009.
[22] V. Everett, D. Walter, J. Harvey, M. Vivar, R. Van Scheppingen, S. Surve, A. Blakers, P. Le Lievre, M. Greaves, A. Tanner, A closed loop tracking system for a linear fresnel hybrid PV/thermal micro-concentrator system, in: The 25th European Photovoltaic Solar Energy Conference and Exhibition (25th EU PVSEC)/The Fifth World Conference on Photovoltaic Energy Conversion (WCPEC-5), Valencia, Spain, 2010, pp. 1063–1065.
[23] V. Everett, D. Walter, J. Harvey, M. Vivar, R. Van Scheppingen, S. Surve, A. Blakers, P. Le Lievre, M. Greaves, A. Tanner, Enhanced longitudinal and lateral flux uniformity for linear fresnel reflectors in concentrating photovoltaic systems, in: The 25th European Photovoltaic Solar Energy Conference and Exhibition (25th EU PVSEC)/The Fifth World Conference on Photovoltaic Energy Conversion (WCPEC-5), Valencia, Spain, 2010, pp. 1060–1062.
[24] T. Sultana, G.L. Morrison, G. Rosengarten, Thermal performance of a novel rooftop solar microcon-centrating collector, Sol. Energy 86 (7) (2012) 1992–2000.
[25] D. Walter, V. Everett, M. Vivar, J. Harvey, R. Van Scheppingen, S. Surve, J. Muric-Nesic, A. Blakers, A.W. Bett, R. D. McConnell, et al., A monolithic micro-concentrator receiver for a hybrid PV-thermal system: preliminary performance, in: AIP Conference Proceedings, vol. 1277, 2010, p. 70.
[26] M. Vivar, V. Everett, M. Fuentes, A. Blakers, A. Tanner, P. le Lievre, M. Greaves, Initial field performance of a hybrid cpv-t microconcentrator system, Prog. Photovolt. Res. Appl 21 (8) (2013) 1659–1671.
[27] The Radiant Zemax LLC, Zemax 13. URL ⟨https://www.zemax.com/home⟩, 2013.
[28] N.R.E.L. (NREL), Reference Solar Spectral Irradiance: Air Mass 1.5. URL ⟨http://rredc.nrel.gov/solar/spectra/am1.5/⟩, 2014.
[29] A. Imenes, D. Buie, D. McKenzie, The design of broadband, wide-angle interference filters for solar concentrating systems, Sol. Energy Mater. Sol. Cells 90 (11) (2006) 1579–1606.
[30] M. Modest, Radiative Heat Transfer, Elsevier Science. URL ⟨http://books.google.com.au/books?id=J2KZq0e4lClC⟩, 2013.
[31] Openfilters, URL ⟨http://larfis.polymtl.ca/index.php/en/links/openfilters⟩, 2014, Montreal, Canada.
[32] S. Larouche, L. Martinu, Openfilters: open-source software for the design, optimization, and synthesis of optical filters, Appl. Opt. 47 (13) (2008) C219–C230.
[33] V. Everett, D. Walter, J. Harvey, M. Vivar, R. Van Scheppingen, S. Surve, A. Blakers, P. Le Lievre, M. Greaves, A. Tanner, A linear fresnel hybrid PV/thermal micro-concentrator system for rooftop integration, in: The 25th European Photovoltaic Solar Energy Conference and Exhibition (25th EU PVSEC)/The Fifth World Conference on Photovoltaic Energy Conversion (WCPEC-5), 2010, pp. 3937–3941.
[34] M. Weber, Handbook of Optical Materials, Laser & Optical Science & Technology, Taylor & Francis, Boca Raton, Florida, U.S, 2002.
[35] A. Mojiri, C. Stanley, E. Thomsen, V. Everett, A. Blakers, G. Rosengarten, A heat transfer model for concentrating silicon solar cells in a spectrally splitting hybrid receiver, in: Proceedings of the 15th International Heat Transfer Conference/IHTC-15, Tokyo, Japan, 2014, http://dx.doi.org/10.1615/IHTC15.sol.009067.
[36] C. Stanley, A. Mojiri, N. Karwa, G. Rosengarten, Thermal performance analysis of a concentrating beam splitting hybrid PVT collector, in: EuroSun 2014, AIX-LES-BAINS, France, 2015.